Molecular dynamics simulation of vibrational relaxation of highly excited molecules in fluids. II. Nonequilibrium simulation of azulene in CO 2 and Xe

C. Heidelbach, V. S. Vikhrenko, D. Schwarzer, and J. Schroeder

Citation: The Journal of Chemical Physics **110**, 5286 (1999); doi: 10.1063/1.478423
View online: http://dx.doi.org/10.1063/1.478423
View Table of Contents: http://scitation.aip.org/content/aip/journal/jcp/110/11?ver=pdfcov
Published by the AIP Publishing

Molecular dynamics simulation of vibrational relaxation of highly excited molecules in fluids. II. Nonequilibrium simulation of azulene in CO_2 and Xe

C. Heidelbach, V. S. Vikhrenko,[a] D. Schwarzer, and J. Schroeder
Max-Planck-Institut für Biophysikalische Chemie, Am Fassberg 11, D-37077 Göttingen, Germany

(Received 13 August 1998; accepted 15 December 1998)

Results of nonequilibrium molecular dynamics simulations of vibrational energy relaxation of azulene in carbon dioxide and xenon at low and high pressure are presented and analyzed. Simulated relaxation times are in good agreement with experimental data for all systems considered. The contribution of vibration–rotation coupling to vibrational energy relaxation is shown to be negligible. A normal mode analysis of solute-to-solvent energy flux reveals an important role of high-frequency modes in the process of vibrational energy relaxation. Under all thermodynamic conditions considered they take part in solvent-assisted intramolecular energy redistribution and, moreover, at high pressure they considerably contribute to azulene-to-carbon dioxide energy flux. Solvent-assisted (or collision-induced) intermode energy exchange seems to be the main channel, ensuring fast intramolecular energy redistribution. For isolated azulene intramolecular energy redistribution is characterized by time scales from several to hundreds of ps and even longer, depending on initial excitation. The major part of solute vibrational energy is transferred to the solvent via solute out-of-plane vibrational modes. In-plane vibrational modes are of minor importance in this process. However, their contribution grows with solvent density. The distribution of energy fluxes via azulene normal modes strongly depends on thermodynamic conditions. The contribution of hydrogen atoms to the overall solute-to-solvent energy flux is approximately two to three times higher than of carbon atoms depending on the system and thermodynamic conditions as well. Carbon atoms transfer energy only in the direction perpendicular to the molecular plane of azulene, whereas hydrogen atoms show more isotropic behavior, especially at high pressure. [S0021-9606(99)51311-1]

I. INTRODUCTION

Nonequilibrium molecular dynamics (MD) simulations of vibrational energy relaxation (VER) of small size molecules in fluids have been shown[1–3] to be an important source of information about the detailed dynamics of such processes. The methods for extracting this information from simulation data on moderate size solutes were described in the preceding paper,[4] hereafter referred to as I.

Our work is mainly concerned with those features of VER that are not easily accessible by current experimental techniques. We use principle axes and Eckart molecular frames for decoupling rotational and vibrational motion to investigate the role of solvent rotation and translation and the significance of vibration–rotation interaction. The connection between molecular spectra and structure and VER can be understood by considering the ''fine structure'' of vibrational energy flux, i.e., how the solvent-to-solute energy flux is distributed among the normal modes or atoms of the solute. Another central point that we address is intramolecular vibrational energy redistribution (IVR) in the isolated and solvated solute molecule.

In selecting a suitable system for simulations we have taken into account that azulene belongs to a class of intensively studied substances and many experimental data are available[5–14] on VER of azulene in different solvents under various thermodynamic conditions. Carbon dioxide is a solvent environment of great interest due to its widespread use in supercritical extraction and much data from experimental[15,16] and theoretical[17–19] investigations are available, too. Xenon, in contrast to carbon dioxide, is a monoatomic fluid that may also be used for experimental studies covering wide density ranges. Hence, interesting information can be derived from comparing the behavior of azulene in these two qualitatively different solvents. For a long time xenon was considered as a standard system for the construction of liquid and solid state theories,[20–22] and its properties have been investigated in detail.

The paper is organized in the following way. After a short description of the models used, in Sec. III we discuss similarities and differences between the total energy transfer from excited azulene to carbon dioxide and xenon at low and high pressure. The role of solute rotational and translational degrees of freedom is also considered here. A detailed analysis of the energy flux from solute to solvent in terms of normal mode contributions is given in Sec. IV. The next section is devoted to a study of the behavior of an isolated azulene molecule to reveal the influence of solvent–solute interaction on solute IVR. The distribution of energy flux

[a]Permanent address: Belarussian State Technological University, 13a Sverdlova Str., 220 630 Minsk, Belarus.

among azulene atoms is analyzed in Sec. VI. General conclusions derived from the nonequilibrium simulations are presented in the final part of the paper.

II. DESCRIPTION OF THE MODEL

The model for azulene and CO_2 used in this paper and the details of the simulation were described recently[23] and only the main characteristics are summarized here. In general, we use classical NEV molecular dynamics simulations, treating both the solute and solvent as flexible. The simulation box consists of one azulene molecule surrounded by a bath with periodic boundary conditions. Short-range interactions were truncated at half the box length, whereas long-range electrostatic forces were calculated via the Ewald sum. The time step of integration was chosen as 0.5 fs. All simulations were performed within the CHARMM package,[24] which we modified to our needs.

The azulene potential we used corresponds to *model b* in Ref. 23. It includes harmonic contributions from stretches, bends, and improper torsions, and a cosine dependence on dihedral angles. The potential parameters were tuned to reproduce experimental vibrational frequencies in vacuum. The table of calculated frequency assignments in accordance with the symmetry of azulene normal modes and their comparison with experimental data is given in Ref. 25. The initial solute temperature was adjusted to match experimental conditions[11,12] $\sim$1100 K and the energy flux from azulene to the bath was sampled every 4 fs.

For the azulene–CO_2 system the number of bath molecules was 216 and 337 for low ($\sim$3.2 MPa, $T\cong 445\,\mathrm{K}$, $\rho = 0.93\,\mathrm{mol/l}$) and high pressure ($\sim$270 MPa, $T\cong 298\,\mathrm{K}$, $\rho = 28.7\,\mathrm{mol/l}$), respectively, where T and ρ denote the equilibrium solvent temperature and density at the beginning of the simulation. The CO_2 intramolecular potential was chosen in the form that takes into account stretch, bend, and stretch–stretch harmonic interactions, whereas the intermolecular potential was of an exponential-r^{-6} form in combination with a Coulomb term for atomic charge interactions.[17,18] Parameters and charges for the intermolecular interactions were adjusted to reproduce experimental bulk diffusion and viscosity coefficients at the respective thermodynamic conditions.[19] The azulene–CO_2 interaction was modeled by a 6–12 potential and atom–atom Coulomb interactions, with pressure-independent parameters taken from the QUANTA database.[26] Because of the differences in cooling rates, simulations were carried out for a trajectory length of 263 and 33 ps at low and high pressure, respectively. We generated 40 trajectories for high and 20 for low pressure in order to calculate the required averages; the number of trajectories at 3.2 MPa was limited by computer time and storage requirements.

For the azulene–xenon calculations, the number of bath molecules was 444, independent of pressure. For this system, simulations were performed at 9.0 MPa ($T\cong 295\,\mathrm{K}$, $\rho = 13.0\,\mathrm{mol/l}$) and 200 MPa ($T\cong 295\,\mathrm{K}$, $\rho = 23.3\,\mathrm{mol/l}$), respectively. Xenon–xenon interactions were calculated from the ASM-AT potential[27] as

$$V(r) = V_p(r) + V_{\mathrm{AT}}(r) + V_{sr}(r), \tag{1}$$

TABLE I. Potential parameters of the Xe–Xe interaction.

α^*	5.416 370 17	A_1	428
β^*	4.948 619 34	A_2	33100
A^*	21 058.298	C_9^*	0.108 83
C_6^*	1.028 717 48	$\tilde{D}$	1.18
C_8^*	0.576 558 12	x_1	0.906
C_{10}^*	0.431 846 85	r_m/Å	4.3617
D	1.45	$(\epsilon/k)/K$	282.29

where r is the separation between two xenon atoms and $V_p(r)$ is the HFD-B potential,[28]

$$V_p(r) = \epsilon\left\{ A^* \exp\left[-\alpha^* \frac{r}{r_m} + \beta^* \left(\frac{r}{r_m} \right)^2 \right] - F\left(\frac{r}{r_m} \right) \sum_{j=0}^{2} \frac{C_{2j+6}^*}{(r/r_m)^{2j+6}} \right\}, \tag{2}$$

with

$$F(x) = \begin{cases} \exp\left[-\left(\dfrac{D}{x} - 1 \right) \right]^2, & x < D, \\ 1, & x \geqslant D. \end{cases} \tag{3}$$

$V_{\mathrm{AT}}(r)$ is the so-called Axilrod–Teller correction, which accounts for three-body interactions in terms of a pair potential:

$$V_{\mathrm{AT}}(r) = \epsilon \frac{C_9^*}{x^9} \tilde{F}(x), \quad x = \frac{r}{r_m}. \tag{4}$$

$\tilde{F}(x)$ possesses the same functional form as $F(x)$ but with a different parameter $\tilde{D}$. In addition to this, a short-range correction $V_{sr}(r)$ is included to minimize deviations from the experimental pressure–density curve:

$$V_{sr}(r) = \begin{cases} -\epsilon[A_1(x_1 - x)^3 + A_2(x_1 - x)^6], & x < x_1, \\ 0, & x \geqslant x_1. \end{cases} \tag{5}$$

All potential parameters are given in Table I. As the ASM-AT potential is known to reproduce the pressure–density dependence of pure xenon almost perfectly, no further adjustment of these parameters was necessary.

For the description of the azulene–xenon interaction we used the potential described by Clarke *et al.*,[29] consisting of a 6–12 Lennard-Jones part in combination with a charge-induced dipole interaction to account for the high polarizability of the xenon atoms:

$$V(r) = \frac{A}{r^{12}} - \frac{B}{r^6} - \frac{C}{r^4}, \tag{6}$$

with $A = 3.4440 \times 10^6\,\mathrm{kcal\,Å^{12}/mol}$, $B = 1.2979 \times 10^3\,\mathrm{kcal\,Å^6/mol}$ for all carbon, and $A = 1.1273 \times 10^6\,\mathrm{kcal\,Å^{12}/mol}$, $B = 5.5521 \times 10^2\,\mathrm{kcal\,Å^6/mol}$, and $C = 0$ for all hydrogen atoms. Parameter C for the carbon–xenon interaction depends on the position of the atom in azulene. For atoms[23] 1–6, C was taken equal to[29] 34.161, 46 450, 11.250, 326.36, 3.0396, 262.63 (all numbers have to be multiplied by 10^{-4})

TABLE II. Experimental and calculated values of the vibrational relaxation time (in ps) of azulene in carbon dioxide and xenon at low- and high-pressure conditions.

Solvent	CO_2		Xe	
Pressure (MPa)	3.2	270	9.0	200
Density (mol/l)	0.93	28.7	13.0	23.3
Experimental (Ref. 11) τ	213	18.7	124	86
Calculated τ	306	12.5	265	84.4

kcal $Å^4$/mol, respectively. For both thermodynamic states 40 trajectories of 133 ps length were simulated to obtain the required averages.

III. CHARACTERISTICS OF THE TOTAL ENERGY DECAY AND CONTRIBUTION OF VIBRATION–ROTATION INTERACTION TO THE ENERGY FLUX

The procedure and some results of MD simulations of azulene vibrational energy relaxation in carbon dioxide at low and high pressure were described in Ref. 23. Here, using the methods of analysis developed in I, we give a more detailed analysis of the azulene energy decay through vibrational and rigid body (translational and rotational) degrees of freedom and compare energy transfer mechanisms in carbon dioxide and xenon.

In spite of the fact that general features of the energy decay of azulene are the same in CO_2 and Xe, i.e., exponential decay, an increase of the relaxation rate with solvent density, fast subpicosecond decay of rotation–translation azulene energy, negligibly small contribution of vibration–rotation coupling to VER, quantitative differences appear in the characteristics.

In Table II we present experimental and simulation results for VER times. Generally, in Xe relaxation times are much longer than in CO_2. One should note that while the density of Xe at 9 MPa is as much as 14 times higher than that of CO_2 at 3.2 MPa, the relaxation times are comparable under these conditions. At almost equal densities at high pressure the relaxation times differ by a factor of almost 5 (according to the experimental data) or 7 (MD simulations) times. This acceleration of VER in CO_2 is probably caused by the long-range Az–CO_2 Coulomb interaction as well as by the rotational and internal degrees of freedom of CO_2. The enhancement of energy transfer rates with increasing of the complexity of solvent molecules has been well known experimentally.[11] It seems to be established now[1,3] that Coulomb interactions play an important role in the vibrational energy relaxation of small size molecules, and the relaxation time decreases with its strength.

Due to remaining noise on the simulated trajectories, one obtains slightly different values for the relaxation time depending on the method of their evaluation. Values reported in Table II were obtained by exponential fitting without constraints on the parameters. However, for long times the approximating curves show a considerable amount of equilibrium solute temperature in excess of the solvent. For example, for Az–CO_2 at high pressure the fitted long time limit of kinetic energy is about 380 K, whereas the solute temperature in this limit was estimated to 315 K. Exponential fitting to the simulation data under the constraints of the correct equilibrium temperature results in an increase (except for low-pressure carbon dioxide) of relaxation times: 19.1 ps for CO_2 at high pressure and 106 and 286 ps for Xe and high and low pressure, respectively. In general, the time behavior of azulene vibrational kinetic energy gives reasons to suggest that, within our model, at higher solvent densities a slowing down of relaxation rates is observed when the solute temperature becomes lower.

An important question for the understanding of energy transfer processes during chemical reactions is the role of the rigid body translational and rotational degrees of freedom in energy exchange. As discussed in I, there is no unambiguous way to separate rotations and vibrations in the dynamics of flexible bodies. The most widely used rigid body molecular frames are the Eckart and the principle axes frames. For both frames our calculations indicate no substantial differences in the behavior of rotational and translational energies during VER. Therefore, we discuss in detail only results for the Eckart frame.

In Fig. 1 the time dependence of the total and vibrational energy of azulene in carbon dioxide at high pressure is shown. As discussed earlier,[23] at first, the total energy sharply decreases on a subpicosecond time scale. However, the vibrational energy does not exhibit such a behavior. The difference between the total and the vibrational energy remains almost constant and corresponds to the equilibrium kinetic energy of six rigid body degrees of freedom at an ambient solvent temperature after a very short subpicosecond period mentioned.

The inserts in Fig. 1 show the behavior of rotational and translational energy on 1 and 10 ps time scales, proving that the rigid body degrees of freedom are in thermal equilibrium with the ambient solvent during VER, except for a subpicosecond initial period. Exponential fits to the initial rotational and translational energy decays led to approximately the same relaxation times of about 0.1 ps. For the Az–Xe system rotational and translational energy relaxation times were estimated to about 0.5 and 0.8 ps at 200 MPa and 2.5 and 1.2 ps at 9 MPa, respectively.

The initial time dependence of rotational and translational energy is attributed to the procedure[23] used to prepare the initial state. Before the start of each nonequilibrium simulation the center of mass and rotational velocities of azulene are taken corresponding to the equilibrium solvent temperature, whereas its internal degrees of freedom are ''heated up'' to ~1100 K. During the subsequent equilibration period of 5 ps when azulene is allowed to move while the positions of solvent atoms are kept fixed, its energy redistributes between internal and rigid body degrees of freedom. At high solvent density strong solute–solvent interaction leads to a flux of the excess internal energy of azulene to its rigid body degrees of freedom so that at the end of the equilibration period the energy of rotation and translation of azulene corresponds to the vibrational temperature. On the other hand, at low solvent densities azulene experiences only a few collisions with solvent molecules and almost conserves

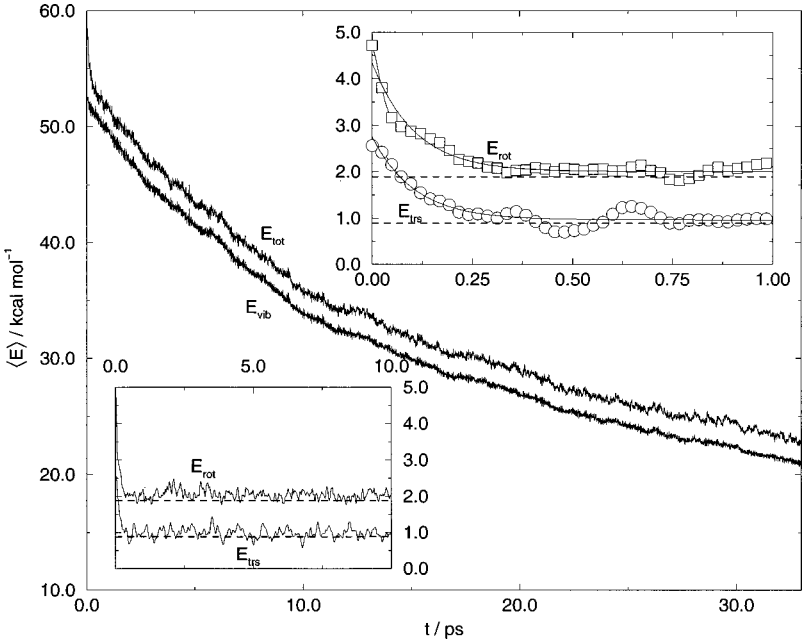

FIG. 1. Total and vibrational energy decay for azulene in carbon dioxide at high pressure. Inserts show the dynamics of rotational and translational energy (for Eckart molecular frame) on 10 and 1 ps time scales. Smoothed curves in the latter insert are the monoexponential fits to corresponding simulation data. Rotational energy curves are shifted upward by 1 kcal/mol. Equilibrium kinetic energy for three degrees of freedom is equal to 0.89 kcal/mol and is shown by dashed lines in the inserts.

its energy. Hence, its rigid body degrees of freedom keep the equilibrium temperature of the box.

Although the excitation of rotations and translations of azulene at high densities is clearly an artefact of initial state preparation, it does not affect VER due to fast subpicosecond loss of the corresponding excess energy, whose dynamics can be analyzed at the same time. Energy exchange between solute rigid body and solvent degrees of freedom should be considered as very effective because corresponding relaxation times are approximately two order of magnitude shorter than VER relaxation times. This conclusion agrees with findings[7,30] from trajectory calculations under gas phase conditions.

Still there remains a small excess of the mean kinetic energy of azulene rigid body degrees of freedom with respect to the equilibrium solvent temperature. The mean values of the rotational and translational kinetic energy in Fig. 1 are about 1 kcal/mol, corresponding to a temperature 335 K, whereas the initial temperature of the solvent was 298 K. This 10% excess of rotational and translational kinetic energy of azulene is observed for all systems and decreases to the solvent temperature as azulene loses its overall excess energy. A possible explanation is that intensive vibrational motion of excited solute atoms is transferred back via the solvent to solute rotational and translational degrees of freedom. Of course, this flux of solute vibrational energy to its rotational and translational degrees of freedom has nothing in common with the widely discussed[31] vibration–rotation interaction, because in the case under discussion the ambient solvent is a necessary transmitter of energy. The contribution of vibration–rotation interaction to vibrational energy redistribution and the role of solvent assisted energy redistribution of solute energy between its vibrational degrees of freedom is discussed in more detail below.

In the case of strong vibration–rotation interaction an appreciable amount of energy can be transferred via this channel even if rotational motion of the solute will almost be in thermal equilibrium with the solvent. Hence, the energy flux from vibrational to rotational solute degrees of freedom has to be analyzed. Different rotation–vibration coupling terms arise depending on the coordinate frame chosen.[4] For the Eckart frame there are four different channels of interaction between rotations and vibrations:

$$N_{1\mathrm{v\ r}} = \tfrac{1}{2}\boldsymbol{\omega}' \cdot \dot{\mathbf{I}} \cdot \boldsymbol{\omega}', \tag{7}$$

$$N_{2\mathrm{v-r}} = \frac{d}{dt}\left(\frac{\boldsymbol{\omega} + \boldsymbol{\omega}'}{2} \cdot \mathbf{I} \cdot \Delta\boldsymbol{\omega} \right), \tag{8}$$

$$N_{3\mathrm{v-r}} = \frac{d}{dt}(\boldsymbol{\omega} \cdot \mathbf{L}_{\mathrm{vib}}), \tag{9}$$

$$N_{4\mathrm{v-r}} = -\mathbf{M}_C^{(e)} \cdot \Delta\boldsymbol{\omega}, \tag{10}$$

where ω and ω' are the angular velocities of Eckart and instantaneous principle axes frames, respectively, $\mathbf{I}$ is the moment of inertia tensor, and $\dot{\mathbf{I}}$ the respective time derivative. $\Delta\omega$ denotes the difference between the angular velocities of the Eckart and the principle axes frames, while $\mathbf{L}_{\mathrm{vibr}}$ stands for the angular momentum of the vibrational motion in the Eckart frame. The last term includes the torque of the external forces, $\mathbf{M}_c^{(e)}$. The first channel is connected to variations in instantaneous moments of inertia; the second one is due to differences between the angular velocities of the Eckart frame and the system of principle axes. The third coupling term is caused straightforwardly by the vibrational velocities and the last one is attributed to interactions with the solvent. Integration in time of these coupling capacity terms results in the energy transferred through the respective channels.

As an analytical estimation of these contributions is difficult for a complex system like azulene, we evaluated these terms directly in the course of the energy transfer simulations. In Fig. 2 integrals over time of the corresponding capacities are plotted. These integrals can be interpreted as

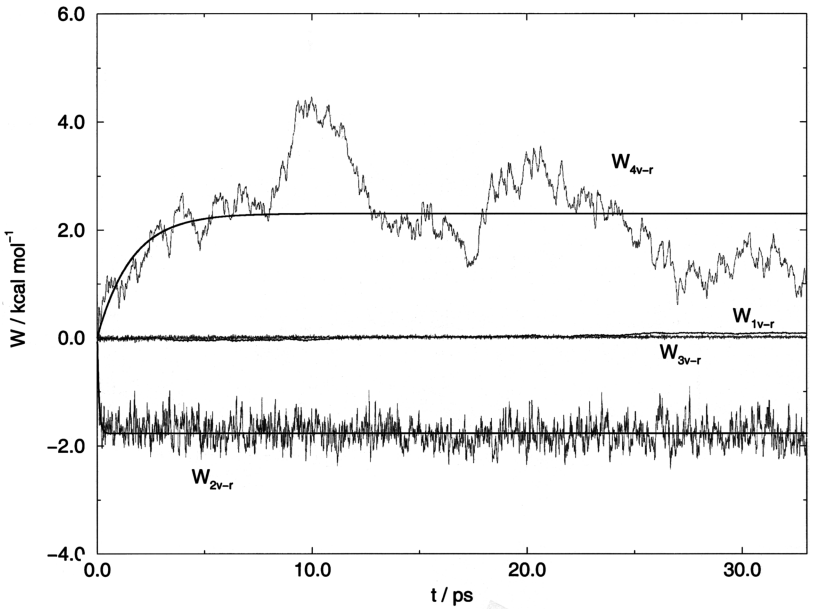

FIG. 2. Cumulative (after integration of capacities over time) energy exchange between vibrational and rotational degrees of freedom of azulene in carbon dioxide at high-pressure conditions calculated for the Eckart frame. Subscripts at W indicate energy exchange channels according to Eqs. (7)–(10). W_{1v-r} represents the vibrational–rotational energy exchange for the principle axes frame, too.

energies W transferred from vibrational to rotational solute degrees of freedom due to rotation–vibration coupling. Channels 1 and 3 are of minor importance (the contribution of channel 1 amounts to less than 0.3% of the total energy transferred). The main contributions arise from the second and fourth channels. Both contributions are proportional to the difference between angular velocities of Eckart and principle axes frames. Their relaxation constants are about 0.085 and 1.6 ps, respectively, and the total contribution over all the channels is rather small. Cumulative energy exchange via the second channel is negative, i.e., it looks like energy goes from rotations to vibrations. After a short initial adjusting period of an order of 1 ps mean values of capacities characterizing vibration–rotation coupling become negligibly small. This supports the conclusion that vibration–rotation coupling as a channel of energy exchange during VER can be safely neglected.

The Eckart frame is suitable for harmonic vibrational analysis because its definitions,[32] (2.9) and (2.11) of I are linear expressions. However, this frame is not natural for a general dynamic description of a many-body system due to the nonzero intrinsic angular momentum and a more complicated equation of rotational motion as compared to the principle axes frame. For the latter only the first channel [Eq. (7)] of vibration–rotation interaction arises (see I), again resulting in a negligible contribution to VER.

The same qualitative picture is observed for vibration–rotation coupling in VER of azulene in xenon, though the numerical values of the different channels slightly differ. One may conclude, therefore, that in spite of the fact that rotational motion cannot be rigorously separated from vibrations and the discussion of vibration–rotation coupling is ambiguous to some extent, the results for two different molecular frames and two different solvents suggest that the solute vibrational energy $E_{1\mathrm{vib}}$ is dissipated directly through interactions between the vibrational modes of azulene and the solvent, independent of the structure of the bath molecules and the molecular frame chosen.

IV. NORMAL MODE ANALYSIS OF THE SOLUTE-TO-SOLVENT ENERGY FLUX

MD simulations give us the possibility to describe and analyze such details of the energy flux as its distribution among the normal modes or atoms of the solute. As there were no essential differences observed between results for Eckart and principle axes frames, our analysis can be restricted to the Eckart frame without loss of generality.

In view of the results of the previous section, the vibration–rotation coupling capacities in Eq. (2.25) of I can be omitted. Then the time derivative of the solute vibrational energy $E_{1\mathrm{vib}}$ is defined only by the external forces $\mathbf{F}_i^{(e)}$ imposed on the solute nuclei i by the solvent

$$\frac{dE_{1\mathrm{vib}}}{dt}=\sum_{i=1}^{n}\mathbf{u}_i\cdot\mathbf{F}_i^{(e)}, \tag{11}$$

where $\mathbf{u}_i$ is the vibrational velocity of nucleus i defined by

$$\mathbf{u}_i=\mathbf{v}_i-\mathbf{v}_C-\boldsymbol{\omega}\times\mathbf{r}_{iC}, \tag{12}$$

$\mathbf{v}_i$ is the velocity of nucleus i in the laboratory frame, $\mathbf{v}_C$ is the solute center of mass velocity, $\mathbf{r}_{iC}$ is the position vector of the ith nucleus in the center of mass frame and $\boldsymbol{\omega}$ is the rotational velocity of the Eckart frame (for a description of how to construct the latter, see Ref. 33).

With the help of the orthonormalized transition matrix $\mathbf{P}_{\alpha i}$ calculated from the normal mode analysis of the isolated azulene molecule, normal mode velocities $\dot{q}_\alpha$ and external forces $Q_\alpha^{(e)}$ are introduced:

$$\dot{q}_\alpha=\sum_{i=1}^{n}\mathbf{P}_{\alpha i}^{t}\cdot\sqrt{m_i}\mathbf{u}_i, \quad \alpha=1,2,...,3n-6, \tag{13}$$

$$Q_\alpha^{(e)}=\sum_{i=1}^{n}\mathbf{F}_i^{(e)}\cdot\frac{1}{\sqrt{m_i}}\mathbf{P}_{i\alpha}. \tag{14}$$

The rhs of Eq. (11) is bilinear in velocities and forces. Therefore, it can be identically represented by external nor-

mal forces and normal mode velocities, and the equation describing the evolution of the internal vibrational energy attains the form

$$\frac{dE_{1\,\mathrm{vibr}}}{dt}=\sum_{\alpha=1}^{3n-6}\dot{q}_\alpha\cdot Q_\alpha^{(e)}. \tag{15}$$

The capacities $\dot{q}_\alpha\cdot Q_\alpha^{(e)}$ can be interpreted as the energy exchange rate between the solute and solvent via particular mode α. The total energy transferred from the solute via the αth mode in the time interval t_1-t_0 is defined by the integral

$$W_\alpha=-\int_{t_0}^{t_1}\dot{q}_\alpha Q_\alpha^{(e)}\,dt. \tag{16}$$

The model of azulene intramolecular interactions is harmonic (except of small anharmonicities on dihedral angles) in internal (or natural intramolecular) coordinates. However, the derivation of the equations of motion requires us to rewrite the kinetic energy, which is harmonic in Cartesian coordinates, in the same intramolecular coordinates or, *vice versa*, to rewrite the potential energy in Cartesian coordinates. The transition matrix between these two coordinate systems is strongly nonlinear. Hence, even a harmonic (in internal coordinates) intramolecular potential results in nonlinear equations of motion.

Our normal mode analysis is based on Cartesian coordinates. Thus, the normal mode representation of the kinetic energy is exact. However, the representation of the potential energy may become very inaccurate,[33] especially for large differences between the force constants (or vibrational frequencies) of bend and stretch deformations. A qualitative explanation of kinematic nonlinearities and an estimation of the inaccuracy in potential energy due to the Cartesian basis of normal coordinates is given in the Appendix.

The azulene intramolecular potential comprises two-, three-, and four-body interactions. After the transition to normal modes it results in multimode nonlinear coupling terms. In turn, Eqs. (A2)–(A4) of I, which describe the evolution of particular normal modes, include intermode coupling terms, making slightly ambiguous the interpretation of the energy flux to the solvent in terms of the rhs of Eq. (15). Nevertheless, the dominant part of energy exchange between normal mode α and the solvent is described by the normal force capacity $\dot{q}_\alpha Q_\alpha^{(e)}$, and in the following we will analyze the energy flux in terms of these quantities. Correlations between different mode specific energy fluxes will be considered in Ref. 34 on the basis of an equilibrium statistical–mechanical description[4] of VER.

In Fig. 3 the distribution of the energy transferred through a particular mode is plotted versus the mode number (histograms **c** and **d**) for the Az–CO_2 system. As was suggested from classical trajectory calculations,[7,9,30] at low pressure the main part of energy (about 80%) is dissipated through the five lowest-frequency modes. At high pressure, however, this behavior changes significantly. Here only 30% of the energy is transferred through these modes. This difference between low- and high-pressure data is even more pronounced in curves **a** and **b** in Fig. 3, which show the accumulated energy transfer by all modes $i\leqslant n$ vs n.

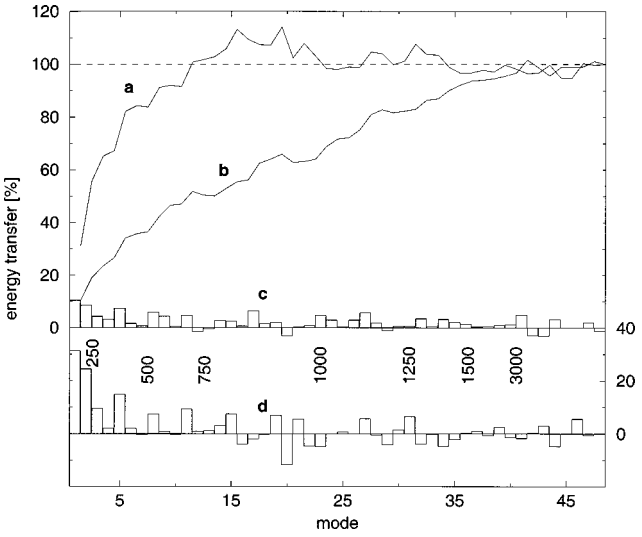

FIG. 3. The normal mode distribution of energy flux for an Az–CO_2 system at low [curve (a) and histogram (d)] and high [curve (b) and histogram (c)] pressure. Histograms show the distribution of energy flux among individual modes whereas curves represent cumulative energy transfer by all lower number modes. For comparison, some frequencies (in cm^{-1}) are indicated along the abscissa. A big gap exists between the highest ring ($\omega_{40}=1542\ cm^{-1}$) and the lowest C–H stretch ($\omega_{41}=3028\ cm^{-1}$) frequencies.

It is interesting to note that some modes (e.g., No. 20) gain energy from the solvent. Other modes are almost inactive (Nos. 37, 45). These differences between individual vibrations depend on the structure of the respective normal vectors, geometric and force characteristics of CO_2 molecules, and thermodynamic conditions, which define[23] the mutual azulene–CO_2 space distribution. For mode No. 20 the influence of the geometrical properties of the azulene and bath molecules is so strong that the direction of the solvent-to-solute energy flux remains stable over two orders of magnitude in pressure. The arguments also hold with respect to the inactivity of the modes 37, 45.

To explain this peculiarity one has to resort to the definition of the normal force in Eq. (14). From this equation it is obvious that the external force $\mathbf{F}_i^{(e)}$ acting on solute atom i contributes to a variety of normal forces $Q_\alpha^{(e)}$, depending on the orientation of the respective normal vectors forming the basis of the transition matrix $\mathbf{P}_{i\alpha}$. Thus, in the course of an azulene–CO_2 collision, intramolecular intermode energy exchange occurs, which results in a solvent-assisted IVR. In addition to this, during a collision a CO_2 molecule interacts with several azulene atoms contributing to many normal forces simultaneously.

A complementary explanation of these facts is possible. When a collision between the solute and a solvent molecule occurs, a new complex consisting of these two molecules is formed. It is characterized by a new set of normal modes that hybridize different modes of the solute. The evolution of these new modes during the collision period results partially in the redistribution of energy between solute modes and partially in the energy exchange between the solute and solvent. At high densities this effect is even more pronounced due to the presence of complexes consisting of one solute and several solvent molecules.

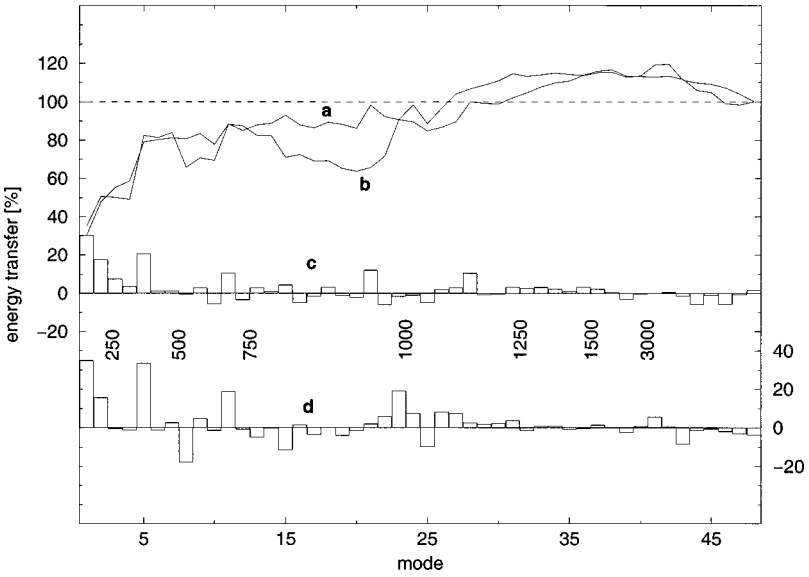

FIG. 4. The same as in Fig. 3, for an Az–Xe system.

In the low-pressure regime many of the high-frequency modes are active. Nevertheless, as indicated in the cumulative energy transfer in Fig. 3, their activity most probably results in intramolecular energy redistribution only. The spectral diapason above 600 cm^{-1} seems to be determined by elastic interactions between Az and CO_2. At 250 MPa, on the other hand, the dense environment apparently has a dissipative effect on the colliding partners and almost all modes contribute to the energy exchange between the solute and solvent. Modes dominated by the elastic part of the solute–solvent interaction can only be found in the spectral diapason of the C–H stretching modes above 3000 cm^{-1}. At neither low nor high pressure there are indications of resonance energy transfer with CO_2 eigenfrequencies[35] (667, 1388, and 2329 cm^{-1}).

While for CO_2 the density change between low and high pressure amounts to a factor of ~30, the density change in Xe is less than a factor of 2. Thus, for the different conditions in Xe a similar decay behavior is expected (Fig. 4). In both thermodynamic states about 80% of the energy is transferred through mode 1–5, which is comparable with the observation in CO_2 at 3.2 MPa. But, while almost the entire energy transfer in low-pressure CO_2 is carried by modes 1–11, in Xe modes up to 30 contribute significantly to the energy exchange. The differences between CO_2 and Xe can be understood by comparing the densities and interaction potentials of the two solvents.

The density of Xe at 200 MPa is 23.3 mol/l and on the same order of magnitude as for CO_2 at 250 MPa ($\rho = 28.7$ mol/l). Nevertheless, the energy transfer mechanism shows significant differences. In xenon the dominance of the low-frequency modes is still pronounced, while in CO_2 the transferred energy raises monotonously over a wide frequency range up to ~1600 cm^{-1}. As in the case of the total energy flux, this discrepancy might be attributed either to the polyatomic structure of carbon dioxide or the long-range Coulomb interactions, which induce long-range solute–solvent coupling, or the accumulation of both effects. This observation is in agreement with calculations,[1,3] which indicate the important influence of the Coulomb forces on energy transfer over the whole frequency range.

A great activity of out-of-plane modes appears in the distribution of energy flux over normal modes of different symmetry shown in Figs. 5 and 6. Here 48 azulene vibrational modes decompose on 6 out-of-plane asymmetric, 9 out-of-plane symmetric, 16 in-plane asymmetric, and 17 in-plane symmetric ones. For Az–Xe at low pressure [Fig. 6(a)] more than 90% of the vibrational energy is transferred by out-of-plane asymmetric vibrations, whereas for Az–CO_2 [Fig. 5(a)] the main part of energy (about 70%) fluxes through out-of-plane symmetric modes. For both systems the contribution of in-plane vibrations to the energy flux is hardly distinguishable from fluctuations.

At high pressure, carbon dioxide enhances all types of energy transfer channels with the dominating role of out-of-plane symmetric vibrations [Fig. 5(b)], whereas in high pressure Az–Xe in-plane vibrations remain almost inactive with respect to energy transfer [Fig. 6(b)].

It is not surprising that the distribution of energy fluxes among the particular normal modes is very sensitive to thermodynamic conditions. The distribution depends on the structure of azulene normal vectors and the distribution of solvent molecules around azulene. As components of normal vectors relating to displacements of Az atoms strongly vary from atom to atom for even low-frequency modes, small changes in solvent spatial distribution functions in the vicinity of the solute will result in a strong redistribution of energy flux between different vibrational modes.

V. MD SIMULATIONS OF ISOLATED AZULENE

In Ref. 25 we have shown that in spite of the almost harmonic azulene intramolecular potential collisions lead to efficient IVR such that the equipartition of energy between different azulene vibrations is maintained during VER. In order to distinguish between intramolecular and solvent contributions to IVR, additional simulations on isolated azulene have been carried out. Again we analyze our classical model

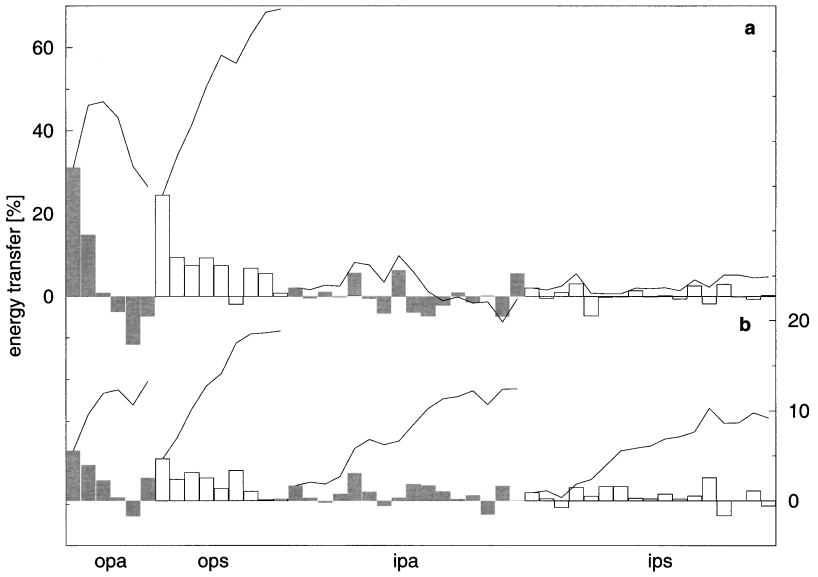

FIG. 5. Symmetry assignment of the normal mode distribution of energy flux for an Az–CO_2 system: (a) low pressure; (b) high pressure. Curves represent the cumulative energy transfer for each symmetry group: out-of-plane asymmetric (opa, modes 1, 5, 9, 16, 20, 23), out-of-plane symmetric (ops, modes 2, 3, 8, 11, 15, 17, 19, 21, 25), in-plane asymmetric (ipa, modes 4, 7, 13, 18, 27, 28, 29, 31, 32, 34, 35, 37, 40, 42, 44, 46), in-plane symmetric (ips, modes 6, 10, 12, 14, 22, 24, 26, 30, 33, 36, 38, 39, 41, 43, 45, 47, 48).

without any attempts to take into account quantum mechanical aspects such as the effect of zero-point energy or the discrete character of the vibrational spectrum.

Initially excited states of azulene were prepared by assigning each vibrational mode α energy corresponding to some temperature T_α in accordance with the harmonic approximation,

$$q_{\alpha 0}=(a_{\alpha 0}/\omega_\alpha)\sin\varphi_\alpha, \quad \dot{q}_{\alpha 0}=a_{\alpha 0}\cos\varphi_\alpha,$$
$$a_{\alpha 0}=\sqrt{k_B T_\alpha}, \tag{17}$$

where φ_α is the random phase. Different initial states were generated by a random choice of φ_α from a uniform distribution. Cartesian vibrational atomic velocities and displacements were calculated by the inversion of Eq. (13) [Eq. (2.36) of I]. This preparation of initial states led to a slightly nonequilibrium distribution of energy due to the overestimation of the potential energy by the harmonic approximation, especially for higher-frequency modes. However, it has no consequences for the estimation of IVR efficiencies.

In a set of additional simulations, all azulene vibrational modes were given the same initial temperature of about 1100 K. The deactivation of azulene was induced by friction forces proportional of velocities of a subset of normal modes,

$$Q_\alpha^{(\mathrm{ef})}=-\mu_\alpha\dot{q}_\alpha, \quad \alpha=1,2,...,k, \tag{18}$$

so that external forces exerted on azulene atoms were calculated by the expression

$$F_i^{(\mathrm{ef})}=-\sqrt{m_i}\sum_{\alpha=1}^{k}\mu_\alpha \mathbf{P}_{i\alpha}\dot{q}_\alpha, \quad i=1,2,...,18, \tag{19}$$

where μ_α are friction coefficients.

It is not possible to cool azulene efficiently when k is taken equal to 1. At small μ_1 the deactivation process is slow due to small friction, whereas at high μ_1 mode 1 is selectively cooled on a subpicosecond time scale and is not able to transfer energy efficiently because of its low velocity. For μ_1 in the diapason[36] 10–400 ps^{-1}, a linear regression gave

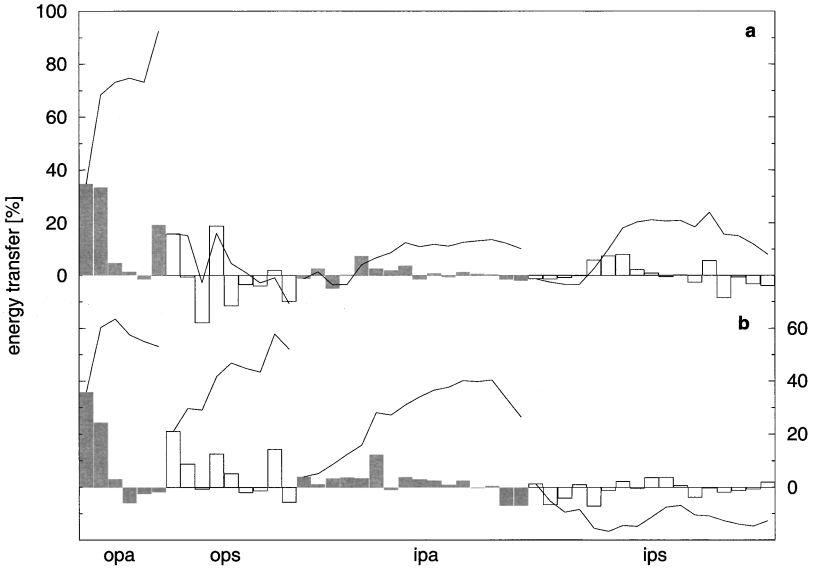

FIG. 6. The same as for Fig. 5, for an Az–Xe system.

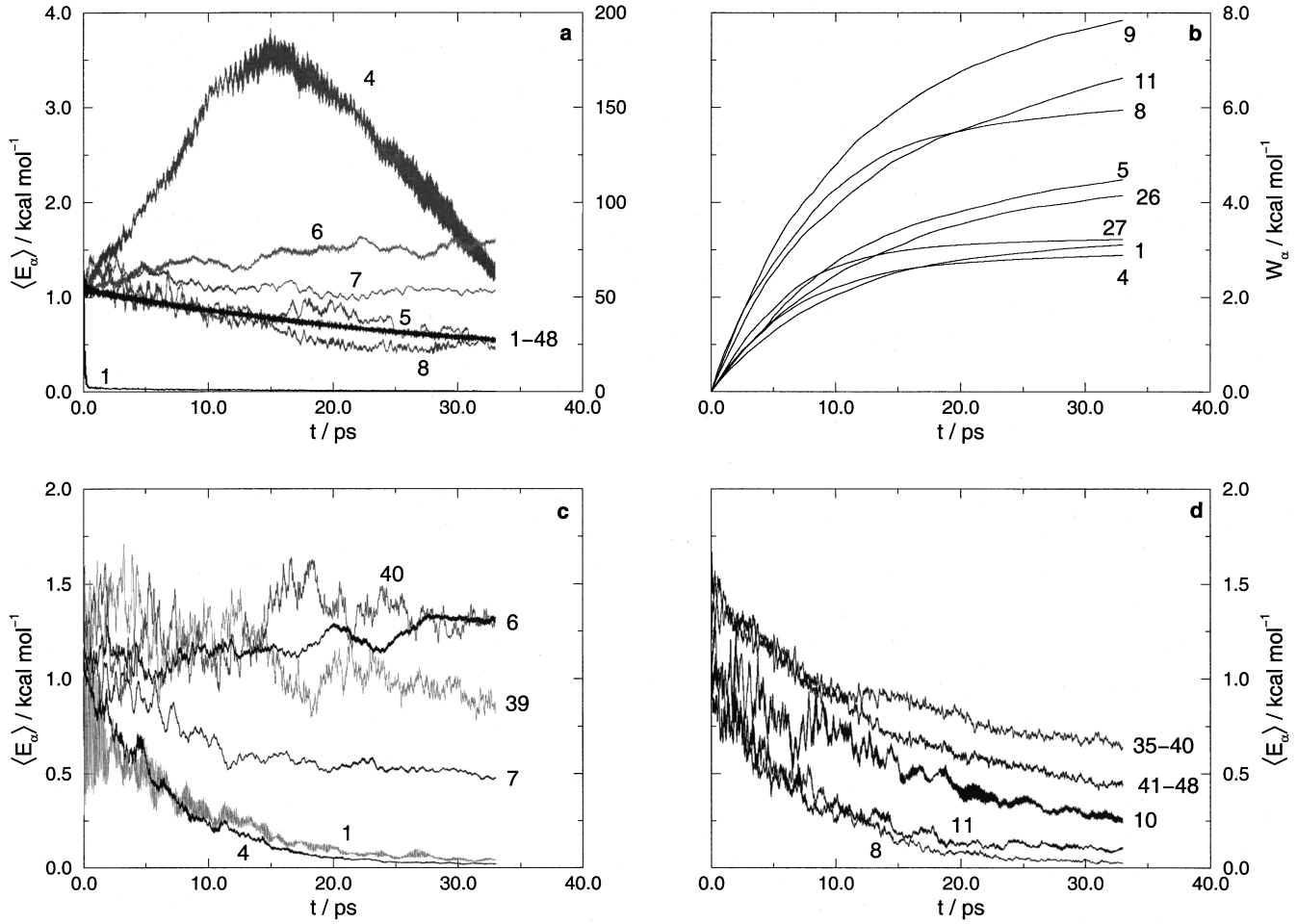

FIG. 7. Intramolecular azulene dynamics under friction forces linear in normal velocities. Mode numbers are indicated in the figures. The time behavior of mode kinetic energies averaged over 50 trajectories and smoothed by a running average is shown. (a). Three lowest modes are damped with the friction coefficient $\mu = 10\ \mathrm{ps}^{-1}$. Decay of the total kinetic energy of modes 1 to 48 is also displayed (the right-hand scale: it approximately coincides with the left-hand scale because curves 1–48 incorporates kinetic energies of 48 modes). b–d. Fifteen modes are damped, as described in the text. Work done by different damping modes is given in (b). The average kinetic energies per high-frequency ring (curves 35–40) and hydrogen mode are displayed in (d) (curves 41–48).

energy decay times of about 140–60 ps weakly dependent on the specific value of μ_1. The distribution of energy between modes during the deactivation was far from equipartition. The long time behavior revealed other relaxation times up to 1000 ps.

A relaxation time of about 30 ps, comparable with cooling rates of azulene in high-pressure carbon dioxide, was achieved at $k=3$ and $\mu_1=\mu_2=\mu_3=\mu=10\ \mathrm{ps}^{-1}$. However, the intramolecular energy distribution was highly nonequilibrium. Results for the time dependence of the kinetic energy for particular modes after averaging over 50 trajectories are shown in Fig. 7(a). The lowest three modes that are affected by friction lose almost all their initial excess energy on a subpicosecond time scale (the energy decay of mode 1 is shown in Fig. 7(a), the energy decays of modes 2 and 3 look similar), whereas modes 4 and 6 gain additional energy, mode 7 almost conserves its energy, and the energy of the other modes decays approximately with the relaxation rate of the total energy. The decays of modes 5 and 8 are shown as examples.

Exponential fitting of the total energy decay curve shows the relaxation time of 33.5 ps. However, the final azulene energy, which is also a fitting parameter, does not equal zero but corresponds to a temperature of 230 K. Biexponential fitting with zero final energy leads to relaxation times of 30 and 200 ps contributing 70% and 30%, respectively. Observed relaxation times for the total energy are mostly independent of the parameters μ and range from 30 to 50 ps for $\mu \in [4{,}160\ \mathrm{ps}^{-1}]$, as estimated from single trajectory simulations.

For $k=4$ and $\mu_1=\mu_2=\mu_3=\mu_4=\mu=16\ \mathrm{ps}^{-1}$ the relaxation time is about 25 ps. The general picture of energy redistribution and transfer in this case is similar to the previous simulations with $k=3$. Despite vibrations 6 and 7, which gain energy, all other modes, with the exception of hydrogen stretches, relax on comparable time scales.

An attempt was undertaken to reproduce VER rates of azulene in high-pressure CO_2. In accordance with the results of Sec. IV (Fig. 3), the most active 15 modes from different spectral regions were subjected to friction. The friction coefficients were taken to prevent the fast collapse of damped vibrations: $\mu=0.2\ \mathrm{ps}^{-1}$ for modes 1–5, $\mu=0.4\ \mathrm{ps}^{-1}$ for modes 8, 9, 11, 17, and 23, and $\mu=0.3\ \mathrm{ps}^{-1}$ for modes 24, 26, 27, 32, and 34. The relaxation time was estimated to be

about 10 ps and long-living high-frequency modes decayed on a time scale of 200 ps. Results after averaging over 50 trajectories are presented in Figs. 7(b),(c),(d).

As shown in Fig. 7(b) the cumulative work done by particular damped modes does not vary strongly. The decreasing slope of these curves indicates a reduction in mode velocities or kinetic energies. These curves are similar to that displayed in Fig. 2 of Ref. 25, except that here the curves are quite smooth. In Figs. 7(c) and 7(d) the behavior of kinetic energies of several modes is shown. The fast decays of modes 1 and 4 correlate with the low cumulative work done by these modes. All damped modes are characterized by a rather fast decay and their kinetic energy curves are located between those of vibrations 4 and 11 shown in Figs. 7(c) and 7(d). Undamped vibrations from modes 12–34 behave like vibrations 7 and 10. All of them show a slow decay after the damped modes have lost their energies. In Fig. 7(d) the average behavior of high-frequency ring (curve 35–40) and hydrogen stretch (curve 41–48) vibrations is shown and underlines their weak energy exchange with other modes. The behavior of modes 6, 39, and 40 [Fig. 7(c)] is mostly untypical, showing almost constant or rising mode energies. This again confirms conclusion about the failure of energy equipartitioning and slow IVR.

Another set of simulations was carried out without any external forces, i.e., for fully isolated azulene. In this set of calculations a group of modes was excited to an initial temperature of 1100 K, whereas all other modes had energies corresponding to 300 K.

When only the high-frequency hydrogen stretch modes 41–48 are excited, their energy is redistributed to other modes on a time scale of about 100 ps. We note that for the case when the energy of all other modes except modes 41–48 is set to zero, almost no energy flux to the other modes is registered. If only mode 45 was excited and the other 47 modes had no initial excitation, the energy was redistributed (not equipartitioned) between hydrogen modes 41, 43, and 47 of the same symmetry (ips) on a picosecond time scale.

The observed energy exchange occurs due to the kinematic nonlinearity, which is qualitatively explained in the Appendix. At zero excitation of the out-of plane modes this nonlinearity is weak and energy exchange is only possible between modes of the same structure and frequency diapason. Initial excitation of lower-frequency modes enables IVR of hydrogen stretch excitations, however, its rate is too low to ensure efficient IVR. Hence, for hydrogen stretch vibrations solvent-assisted IVR is of major importance.

When the in-plane modes 26–40 from the frequency interval 1029–1642 cm^{-1} are excited up to 1100 K while keeping all other modes at 300 K, a relaxation time for IVR of about 5 ps can be estimated to after averaging over 50 trajectories. However, energy decay times for different modes vary and the time behavior of the kinetic energy for some modes is far from exponential. Although in this case IVR is considerably faster in comparison to the case of the excited hydrogen stretches, equipartition of energy is not maintained within the length of trajectories (33 ps) and the relaxation time is substantially longer than a subpicosecond, as commonly assumed. Again, a slowdown of the relaxation process at $t>10$ ps is observed in this set of simulations.

The results of this section are in a sharp contrast to the azulene intramolecular dynamics found in solution, as described in the previous section and in Ref. 25. A remarkably synchronous decay of vibrational energy in the whole azulene spectrum is evident in Fig. 1 of the latter. In this case even the most isolated hydrogen mode 45 shows no difference in behavior from the other modes.

The friction forces introduced in this section have important differences compared to forces exerted by the solvent. At first, they do not contain random components like real solvent forces and hence they do not maintain the vibrational activity of the solute that facilitates intermode energy exchange. Second, they act on each mode separately. As it was discussed earlier, real forces acting on atoms give rise to many normal forces simultaneously, resulting in external energy flux to some modes of the excited solute, and this feature is not modeled by simple frictional forces.

The solvent plays a self-organizing role regulating the intramolecular intermode as well as intermolecular fluxes in such a way that it maintains a quasiequilibrium distribution of solute intramolecular energy, even on the time scale of fast VER of about 10 ps. It effectively assists the redistribution of high-frequency energies, even in our ''classical'' azulene, with an almost harmonic potential and hydrogen stretches that are separated from the other vibrations by a gap of approximately 1500 cm^{-1}. Thus, we may assume that other features of the ''real'' solute such as anharmonicity of the intramolecular potential, zero-point energy, or quantum character of the energy distribution are of minor importance for the description of VER and IVR in solution. We would conclude, therefore, that this highly efficient solvent–solute interaction causing fast energy redistribution, as revealed by our classical MD simulations, yields reasonable results for a classical description of the evolution of highly excited azulene, though one would have expected that quantum effects and anharmonicities are important.

VI. DISTRIBUTION OF THE ENERGY FLUX BETWEEN Az NUCLEI

In analogy to the normal mode analysis in Sec. IV, energy transfer can be discussed on an atomic basis. The vibrational work done by the solute to the solvent then takes the form of the time integral over the rhs of Eq. (11):

$$W_i = -\int_{t_0}^{t_1} \mathbf{u}_i \cdot \mathbf{F}_i^{(e)}\, dt, \tag{20}$$

with W_i being the energy transferred from atom i to the bath. By analyzing the energy dissipation per atom, one can take advantage of the azulene symmetry C_{2v}, in the form that an additional averaging is possible for identical nuclei.

W_i can be divided into an in-plane $W_{i\mathrm{ip}}$ and an out-of-plane $W_{i\mathrm{op}}$ component corresponding to the work done by the external force on atom i along these directions defined by the Eckart frame of the solute,

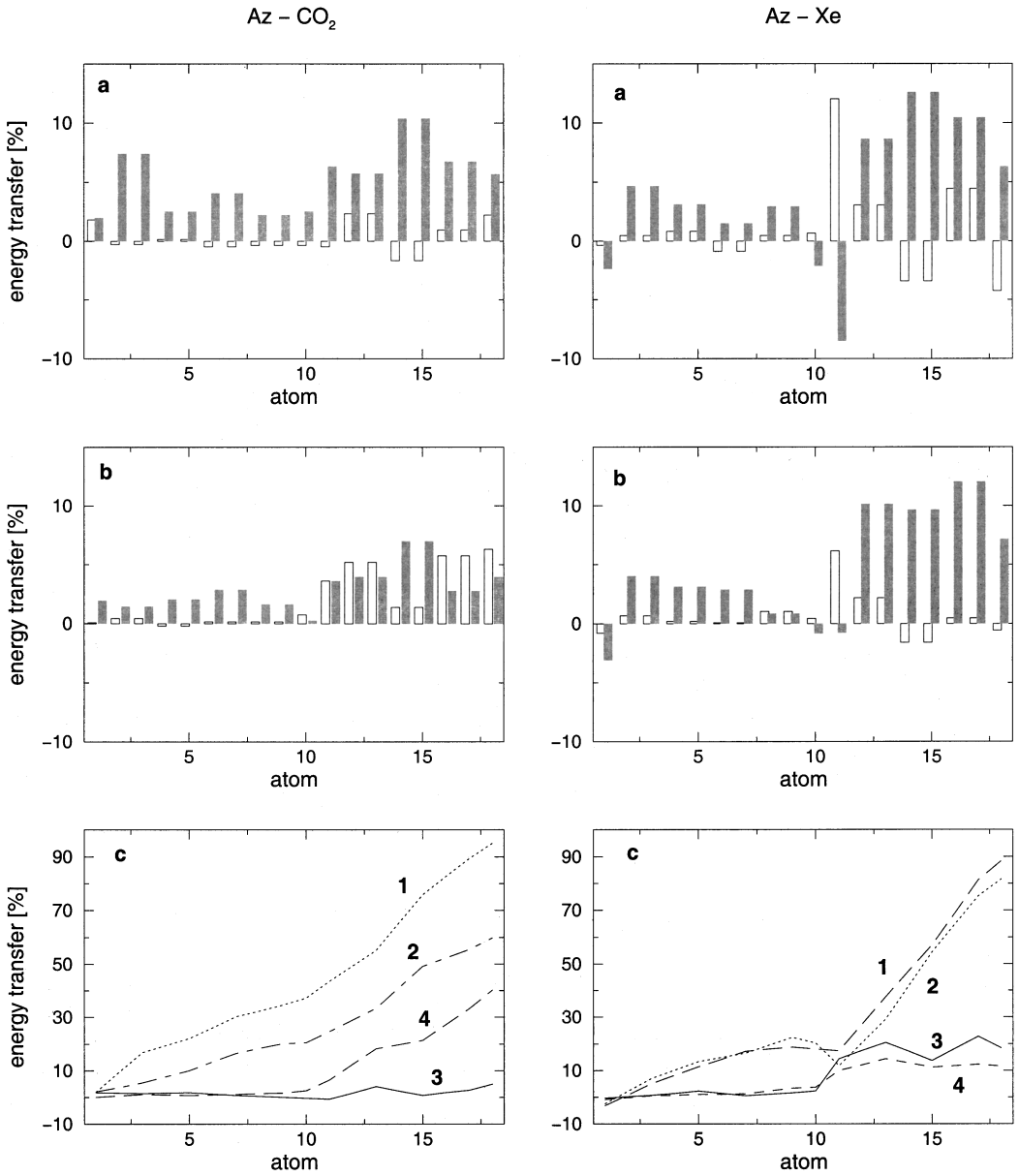

FIG. 8. Atomic distribution of the energy flux for Az–CO_2 (left column) and Az–Xe (right column) systems: (a) low pressure; (b) high pressure; filled and opened columns represent out-of-plane and in-plane contributions, respectively; (c) cumulative over lower number atoms energy flux, curves 1, 3 for low, 2, 4 for high pressure, and 1, 2 for out-of-plane and 3, 4 for in-plane contributions. Carbon atoms are 1–10, hydrogen atoms are 11–18, beginning from the end atoms of the small azulene ring (10th and 18th atoms are the end atoms of the big azulene ring). Assignment of the atoms is given in Ref. 23. Histograms display individual atomic contributions averaged over symmetrically identical pairs of atoms.

$$W_{i\gamma} = -\int_{t_0}^{t_1} \mathbf{u}_{i\gamma} \cdot \mathbf{F}_{i\gamma}^{(e)}\, dt, \quad \gamma \in \{\mathrm{ip,op}\}. \tag{21}$$

The distribution of energy dissipated through a particular atom and the dissipation of the energy by all atoms $i \leqslant n$ is plotted against n for W_i and $W_{i\gamma}$ in Fig. 8.

For CO_2 at low pressure, work is distributed among atoms almost equally while contributions of carbon atoms are different and considerably lower. Practically, all work is done in the out-of-plane direction, which coincides with the results of the normal mode analysis in the previous section. Although many in-plane modes are active their collective contribution almost vanishes.

At high pressure the distribution of work among carbon atoms becomes more homogeneous, the difference between hydrogen and carbon atoms energy transfer increases to approximately a factor of 3. A considerable part of work by hydrogen atoms is done in the molecular plane. This decrease of anisotropy is in correspondence with the cagelike structure[23] enclosing azulene under the given thermodynamic conditions, leading to an almost isotropic environment in the peripheral regions of the solute. Accordingly, the cumulative energy transfer shows a ratio of energy dissipated through carbon to hydrogen atoms of about 20%–80%. The total contribution in the in-plane direction amounts to 40% and is mainly attributed to H atoms, while in the out-of-plane direction 20% of the total energy is transferred by ring and 40% by hydrogen nuclei.

The results for Az–Xe are similar to Az–CO_2 except for

negative work done by the end C atoms at both low and high pressure and a more inhomogeneous distribution between carbon as well as hydrogen atoms, especially at low pressure. Probably, spherical xenon atoms are unable to cover a sufficient area of the azulene surface for smearing up its interaction between different azulene nuclei. Under this assumption structures of normal vectors would influence the atomic work distribution as well.

Azulene interacts with other particles as a system of coupled oscillators and the interaction of individual atoms is mediated by the structure of normal vectors. As a result, the work is smeared between different azulene atoms more or less homogeneously, whereas the distribution between different normal modes is highly inhomogeneous, and even of different signs. Great differences between the efficiency of hydrogen and carbon atoms is explained by much higher deviations of the former from their equilibrium positions (in accordance with the normal vector structure) and a closer contact of hydrogen atoms with the bath. Actually, carbon atoms can interact with the solvent only in the out-of-plane direction.

An additional indication for the importance of the normal mode representation in the investigation of VER caused from the inefficiency of the azulene in-plane degrees of freedom. The in-plane structure of azulene is defined by more rigid bend and stretch bonds, as compared to out-of-plane dihedrals and improper torsions. Hence, its in-plane deformations are rather small and mostly harmonic. This results in almost elastic in-plane collisions. Only at high densities a more complicated interaction with the solvent environment gives rise to a dissipative character of these modes.

VII. CONCLUSION

In this paper we have studied the dynamics of vibrational energy relaxation of an excited azulene molecule in a monoatomic Xe and polyatomic CO_2 solvent. The relaxation rates calculated for different densities in carbon dioxide and xenon by means of nonequilibrium MD simulations are consistent with experimental measurements under similar conditions.

To gain further insight into the details of the transfer mechanism, the energy dissipated from azulene was divided up into translational, rotational, and vibrational contributions. From this separation it was seen that translational and rotational energy relax on a subpicosecond time scale. Moreover, it was shown that vibration–rotation coupling has no importance for the VER, and vibrational energy is transferred directly through interactions between the vibrational subsystem of azulene and the bath.

For the polyatomic solvent (CO_2) with a Coulomb solvent–solute interaction the normal mode analysis has revealed a pronounced difference between the solute–solvent energy exchange mechanism at low and high pressure. For 3.2 MPa the main contributions to the energy flux is attributed to the lowest vibrational modes of azulene, while high-frequency modes show only elastic character. At high pressure, on the other hand, modes from the whole solute spectrum, except the diapason of CH stretches, participate in the VER process with a moderately decreasing contribution with increasing frequency.

In contrast to this, the azulene–xenon system shows almost no pressure dependence in the energy transfer mechanism. At 9 MPa as well as at 200 MPa, about 80% of the energy is transferred through modes 1–5. Nevertheless, vibrations of higher frequencies still maintain a dissipative character of up to $\sim 1500\ \mathrm{cm}^{-1}$ and contribute to the overall energy transfer.

Symmetry analysis has shown that the major part of energy is transferred by out-of-plane vibrations. In-plane vibrations contribute considerably only at high pressure in the $Az-CO_2$ system. The distribution of energy flux on particular normal modes is very sensitive to the thermodynamic conditions especially for Az–Xe, whereas the general picture of cumulative energy flux in this system remains independent of these local variations of the normal mode energy fluxes.

The isolated molecule calculations have demonstrated that solvent-assisted IVR is the key process that maintains energy equipartition between the solute vibrational degrees of freedom (including the most high-frequency hydrogen stretches) during VER and regulates inter- and intramolecular energy fluxes, ensuring monoexponential energy decay.

To complete our analysis, we finally calculated the work done by individual atoms on the solvent. For all systems, the main activity of the carbon atoms in azulene occurs perpendicular to the molecular plane, as expected from simple geometric considerations. For hydrogen atoms, however, the degree of anisotropy is significantly smaller, due to a more homogeneous environment in the peripheral region of the solute molecule.

Differences between the carbon dioxide and xenon systems as well as between low and high pressure have to be interpreted in terms of the spatial distribution of solvent molecules around the solute and more data about this distribution will be necessary for a more detailed analysis of the influence of the solute–solvent structure on energy transfer.

ACKNOWLEDGMENTS

The authors wish to thank Professor Jürgen Troe for continued support. Financial support by the Volkswagen Stiftung (Project No. I70/627) and the Fonds der Chemischen Industrie (for C.H.) is gratefully acknowledged.

APPENDIX: A MODEL OF BEND–STRETCH INTERACTION

We consider a model of bend–stretch interaction. Let l be an equilibrium stretch length and θ and $\lambda = \Delta l/l$ designate intramolecular bend and stretch coordinates (Fig. 9). With corresponding harmonic force constants c_θ and c_λ the kinetic and potential energies of an atom of mass m in the intramolecular (internal) coordinates are represented in a simple form,

$$E_k = \frac{ml^2}{2}[(1+\lambda)^2\dot{\theta}^2 + \dot{\lambda}^2], \tag{A1}$$

$$E_p = \tfrac{1}{2}(c_\theta\theta^2 + c_\lambda\lambda^2). \tag{A2}$$

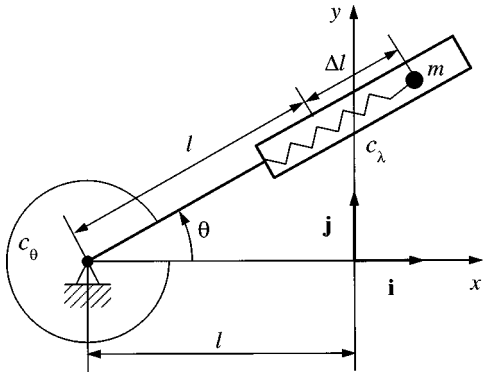

FIG. 9. A model of bend-stretch interaction.

The potential energy is taken as purely harmonic in the internal coordinates. However, nonharmonic contributions connecting bend and stretch vibrations among each other are present in the kinetic energy due to the kinematics of rotational motion. That is why such nonlinearities are called kinematic.

In the harmonic approximation the normal mode frequencies are as follows:

$$\omega_\theta^2 = c_\theta / ml^2, \quad \omega_\lambda^2 = c_\lambda / ml^2, \tag{A3}$$

where stretches usually vibrate with higher frequencies.

As seen from Eqs. (A1) and (A2) for typical stretch deformations $\lambda \leqslant 0.1$, the inaccuracy of the harmonic approximation for energy cannot exceed 20%.

In Cartesian coordinates the kinetic energy is represented by a quadratic form, whereas the potential energy includes nonharmonic contributions,

$$E_k = \frac{ml^2}{2}(\dot{x}^2 + \dot{y}^2), \tag{A4}$$

$$E_p = \frac{1}{2}c_\lambda[y^2 + (1+x)^2 + 1 - 2\sqrt{y^2 + (1+x)^2}] + \frac{1}{2}c_\theta \arctan^2\left(\frac{y}{1+x}\right) = \tfrac{1}{2}c_\lambda(x^2 + xy^2 + \tfrac{1}{4}y^4 + \tfrac{3}{4}x^4 - x^2y^2 + \cdots) + \tfrac{1}{2}c_\theta y^2(1 - 2x + x^2 - 2y^2 + \cdots). \tag{A5}$$

Here coordinates x and y in units of the stretch length l are used.

Normal mode frequencies and normal mode vectors **i** and **j** are the same in internal and Cartesian coordinates, as well. However, the inaccuracy of the Cartesian harmonic approximation for the potential energy,

$$E_{\mathrm{ph}} = \frac{1}{2}(c_\theta y^2 + c_\lambda x^2) = \frac{1}{2}ml^2\omega_\theta^2\left(y^2 + \frac{\omega_\lambda^2}{\omega_\theta^2}x^2\right), \tag{A6}$$

can be quite big depending on the ratio of stretch and bend frequencies. The point is that x can be appreciably different from zero even at zero stretch deformations due to geometrical peculiarities of a bend–stretch structure. Let $\lambda = 0$ and $\theta \neq 0$. Then $y \cong \theta$ and $x \cong -\theta^2/2$ with relative inaccuracy of an order of several per cent at $\theta \leqslant 0.3$, and the expression

$$E_{\mathrm{ph}} \cong E_p\left(1 + \frac{\omega_\lambda^2}{4\omega_\theta^2}\theta^2\right), \tag{A7}$$

for the harmonic potential energy appears. The second term of this expression is nonlinear in internal coordinates and, in reality, it represents an artefact of the harmonic approximation in Cartesian coordinates. A qualitative explanation is that rotation of a stretch bond without its deformation results in a nonzero variation in its Cartesian projection on the equilibrium bond direction. Although this variation is nonlinear in θ, a big deviation is observed for a great difference between the corresponding frequencies. For example, the ratio of the azulene frequencies for hydrogen stretches and lowest torsions or bends is about of 15. Just due to these low-frequency torsion and bend deformations, the deflection of hydrogen stretches from their equilibrium orientations can amount several to tens of degrees. At $\theta \in [0.1, 0.3]$ inaccuracy estimations give values from 50% to 500%. Although a limiting case is considered here, it clearly shows why and how big nonlinear artefacts can appear, when a harmonic Cartesian description of molecular vibrations is used. Of course, these artefacts disappear in higher approximations. Taking only the first three terms in the first parentheses of the series expansion, Eq. (A5), terms of fourth order in θ completely cancel out.

Exact equations of motion can be written either in Cartesian or internal coordinates. For the latter,

$$\ddot{\theta} + \omega_\theta^2\theta = -2(1+\lambda)\dot{\lambda}\,\dot{\theta} - (2+\lambda)\lambda\,\ddot{\theta}, \tag{A8}$$

$$\ddot{\lambda} + \omega_\lambda^2\lambda = (1+\lambda)\,\dot{\theta}^2. \tag{A9}$$

They contain nonlinear terms, which in this simple model can be classified as rotation–vibration coupling Coriolis [the first term on the rhs of Eq. (A8)] and centrifugal [the rhs of Eq. (A9)] forces. The last term in Eq. (A8) characterizes rotation–vibration coupling, too. Making use of successive approximations, we can estimate the rhs's of the equations of motion. The Coriolis force considerably influences the motion of the lower-frequency bending mode because it contains a product of both vibrational frequencies. On the other hand, the centrifugal force in Eq. (A9) is proportional to the square of the bending frequency, however, it is of the zeroth order in small stretch deformation and hence its effect can be comparable to that of the Coriolis force.

Internal motions of different parts of complex molecules contain elements of high-frequency rotations. Hence, for them kinematic nonlinearities also result in terms analogous to rotation–vibration coupling forces. These forces can be sufficiently strong due to high-speed internal rotations.

[1] R. M. Whitnell, K. R. Wilson, and J. T. Hynes, J. Phys. Chem. **94**, 8625 (1990); J. Chem. Phys. **96**, 5354 (1992).
[2] S. Gnanakaran and R. M. Hochstrasser, J. Chem. Phys. **105**, 3486 (1996); P. Hamm, M. Lim, and R. M. Hochstrasser, *ibid.* **107**, 10 523 (1997).
[3] R. Rey and J. T. Hynes, J. Chem. Phys. **104**, 2356 (1996); **108**, 142 (1998).
[4] V. S. Vikhrenko, C. Heidelbach, D. Schwarzer, V. B. Nemtsov, and J. Schroeder, J. Chem. Phys. **110**, 5273 (1999), preceding paper.
[5] D. Schwarzer, J. Troe, and J. Schroeder, Ber. Bunsenges. Phys. Chem. **95**, 933 (1991).
[6] T. Elsaesser and W. Kaiser, Annu. Rev. Phys. Chem. **42**, 83 (1991).

[7] D. L. Clarke and R. G. Gilbert, J. Chem. Phys. **96**, 8450 (1992).
[8] K. Lenz, M. Pfeifer, A. Lau, and T. Elsaesser, Chem. Phys. Lett. **229**, 340 (1994).
[9] R. G. Gilbert, Aust. J. Chem. **48**, 1787 (1995).
[10] G. Lendvay and G. C. Schatz, in *Advances in Chemical Kinetics and Dynamics*, edited by J. R. Barker (JAI, Greenwich, 1995), Vol. 2B.
[11] D. Schwarzer, J. Troe, M. Votsmeier, and M. Zerezke, J. Chem. Phys. **105**, 3121 (1996).
[12] D. Schwarzer, J. Troe, M. Votsmeier, and M. Zerezke, Ber. Bunsenges. Phys. Chem. **101**, 595 (1997).
[13] J. Benzler, S. Linkerdörfer, and K. Luther, J. Chem. Phys. **106**, 4992 (1997).
[14] D. Schwarzer, J. Troe, and M. Zerezke, J. Phys. Chem. A **102**, 4207 (1998).
[15] S. Angus, *IUPAC Chemical Data Series*, No. 7 (Pergamon, Oxford, 1984).
[16] S. Chiappini, M. Nardone, F. P. Ricci, and M. C. Bellisent-Funel, Mol. Phys. **89**, 975 (1996).
[17] S.-B. Zhu and G. W. Robinson, Comput. Phys. Commun. **52**, 317 (1989).
[18] L. M. Nxumalo and T. A. Ford, J. Mol. Struct. **327**, 145, 153 (1994).
[19] I. I. Fedchenia and J. Schroeder, J. Chem. Phys. **106**, 7749 (1997).
[20] J. O. Hirschfelder, C. F. Curtis, and R. B. Bird, *Molecular Theory of Gases and Liquids* (Wiley, New York, 1954).
[21] J. A. Barker, R. O. Watts, J. K. Lee, T. P. Schafter, and Y. T. Lee, J. Chem. Phys. **61**, 3081 (1971).
[22] *Rare Gas Solids*, edited by M. L. Klein and J. A. Venables (Academic, New York, 1976, 1977), Vols. 1, 2.
[23] C. Heidelbach, I. I. Fedchenia, D. Schwarzer, and J. Schroeder, J. Chem. Phys. **108**, 10 152 (1998).
[24] Harvard University, CHARMM 24 b1, 1995.
[25] C. Heidelbach, J. Schroeder, D. Schwarzer, and V. S. Vikhrenko, Chem. Phys. Lett. **291**, 333 (1998).
[26] Molecular Simulation Incorporated, QUANTA 4.0, 1994.
[27] J. H. Kim, T. Ree, and F. H. Ree, J. Chem. Phys. **91**, 3133 (1971).
[28] R. A. Aziz and M. J. Slaman, Mol. Phys. **57**, 825 (1986).
[29] D. L. Clarke, I. Oref, R. G. Gilbert, and K. F. Lin, J. Chem. Phys. **96**, 5983 (1992).
[30] T. Lenzer, K. Luther, J. Troe, R. Gilbert, and K. F. Lim, J. Chem. Phys. **103**, 626 (1995).
[31] E. B. Wilson, Jr., J. C. Decius, and P. C. Cross, *Molecular Vibrations: The Theory of Infrared and Raman Vibrational Spectra* (McGraw-Hill, New York, 1955).
[32] Roman number I refers to expressions in I.
[33] Y. M. Rhee and M. S. Kim, J. Chem. Phys. **107**, 1394 (1997).
[34] C. Heidelbach, V. S. Vikhrenko, D. Schwarzer, I. I. Fedchenia, and J. Schroeder, J. Chem. Phys. (submitted).
[35] G. Herzberg, *Molecular Spectra and Molecular Structure. II. Infrared and Raman Spectra of Polyatomic Molecules* (Van Nostrand Reinhold, New York, 1945).
[36] Frequency of the first mode is 35.6 ps^{-1}. Hence, for this mode being selected from the others vibrational motion can be considered for $\mu_1 \leqslant 71.2\ ps^{-1}$. At $10 \leqslant \mu_1 \leqslant 70\ ps^{-1}$ the damping constant $D_1 = \mu_1/4\nu_1 c$ (where the mode frequency ν_1 is in cm^{-1} and the light velocity c in cm/s) ranges between 0.44 and 31, leading to a fast decay of mode energy during a fraction of the vibration period and motion of this mode is maintained due to a nonlinear interaction with other modes.